J|A|C|S
ARTICLES
Published on Web 03/15/2002

Single-Molecule Magnets: A New Family of Mn_{12} Clusters of Formula $[Mn_{12}O_8X_4(O_2CPh)_8L_6]$

Colette Boskovic,[†] Euan K. Brechin,[†] William E. Streib,[†] Kirsten Folting,[†] John C. Bollinger,[†] David N. Hendrickson,*[,‡] and George Christou*[,†,§]

Contribution from the Department of Chemistry and the Molecular Structure Center, Indiana University, Bloomington, Indiana 47405-7102, and Department of Chemistry 0358, University of California at San Diego, La Jolla, California 92093-0358

Received October 22, 2001

Abstract: The reaction of $(NBu^n_4)[Mn_8O_6Cl_6(O_2CPh)_7(H_2O)_2]$ (**1**) with 2-(hydroxymethyl)pyridine (hmpH) or 2-(hydroxyethyl)pyridine (hepH) gives the $Mn^{II}_2Mn^{III}_{10}$ title compounds $[Mn_{12}O_8Cl_4(O_2CPh)_8(hmp)_6]$ (**2**) and $[Mn_{12}O_8Cl_4(O_2CPh)_8(hep)_6]$ (**3**), respectively, with X = Cl. Subsequent reaction of **3** with HBr affords the Br^- analogue $[Mn_{12}O_8Br_4(O_2CPh)_8(hep)_6]$ (**4**). Complexes **2**·$2Et_2O$·$4CH_2Cl_2$, **3**·$7CH_2Cl_2$, and **4**·$2Et_2O$·$1.4CH_2Cl_2$ crystallize in the triclinic space group $P\bar{1}$, monoclinic space group $C2/c$, and tetragonal space group $I4_1/a$, respectively. Complexes **2** and **3** represent a new structural type, possessing isomeric $[Mn^{III}_{10}Mn^{II}_2O_{16}Cl_2]$ cores but with differing peripheral ligation. Complex **4** is essentially isostructural with **3**. A magnetochemical investigation of complex **2** reveals an $S = 6$ or 7 ground state and frequency-dependent out-of-phase signals in ac susceptibility studies that establish it as a new class of single-molecule magnet. These signals occur at temperatures higher than those observed for all previously reported single-molecule magnets that are not derived from $[Mn_{12}O_{12}(O_2CR)_{16}(H_2O)_x]$. A detailed investigation of forms of complex **2** with different solvation levels reveals that the magnetic properties of **2** are extremely sensitive to the latter, emphasizing the importance to the single-molecule magnet properties of interstitial solvent molecules in the samples. In contrast, complexes **3** and **4** are low-spin molecules with an $S = 0$ ground state.

Introduction

Single-molecule magnets (SMMs) have attracted considerable attention in recent times.[2] Although molecular, these species display superparamagnetic properties normally associated with mesoscale magnetic particles and thus can function as magnetizable magnets below their blocking temperature.[2−4] As a consequence, they represent significant progress in the pursuit of miniaturization of memory storage devices. The SMM behavior results from the intrinsic intramolecular properties of a high-spin ground state and large and negative (easy axis type) magnetoanisotropy, rather than from intermolecular interactions and long-range ordering. Experimentally, the SMM property manifests itself as frequency-dependent peaks in out-of-phase ac susceptibility measurements and as hysteresis loops in magnetization vs dc field studies, the characteristic signatures of superparamagnetic behavior. Furthermore, a number of SMMs have been found to display steps in the hysteresis loops assigned to the presence of quantum tunneling of the magnetization, which emphasizes that these species straddle the classical/quantum interface and provide monodisperse species of nanoscale dimensions for the study of this tunneling phenomenon.[4,5]

To date, the best and most well-studied SMMs are the family of molecules of formula $[Mn_{12}O_{12}(O_2CR)(H_2O)_x]^{n-}$ ($n = 0$, 1, 2; $x = 3$, 4) and their derivatives.[2,3,5−8] However a number of other Mn-containing SMMs are also known: the family of complexes with the $[Mn^{IV}Mn^{III}_3O_3X]^{6+}$ core[4,9] and $[Mn_4(O_2CMe)_2(pdmH)_6]^{2+}$ and the related species $[Mn_4Br_2(H_2O)_2(hmp)_6]^{2+}$ [where $pdmH_2$ is pyridine-2,6-dimethanol and hmpH is 2-(hydroxymethyl)pyridine].[10,11] In addition, Fe- and V-containing SMMs have also been reported: $[Fe_8O_2(OH)_{12}$-

[†] Indiana University.
[‡] University of California at San Diego.
[§] Present address: Department of Chemistry, University of Florida, Gainesville, FL 32611-7200.

(1) Deleted in press.
(2) Christou, G.; Gatteschi, D.; Hendrickson, D. N.; Sessoli, R. *MRS Bull.* **2000**, *25*, 66.
(3) (a) Sessoli, R.; Tsai, H.-L.; Schake, A. R.; Wang, S.; Vincent, J. B.; Folting, K.; Gatteschi, D.; Christou G.; Hendrickson, D. N. *J. Am. Chem. Soc.* **1993**, *115*, 1804. (b) Sessoli, R.; Gatteschi, D.; Caneschi A.; Novak, M. A. *Nature* **1993**, *365*, 141.
(4) Aubin, S. M. J.; Dilley, N. R.; Pardi, L.; Krzystek, J.; Wemple, M. W.; Brunel, L. C.; Maple, M. B.; Christou, G.; Hendrickson, D. N. *J. Am. Chem. Soc.* **1998**, *120*, 4991.
(5) (a) Friedman, J. R.; Sarachik, M. P. *Phys. Rev. Lett.* **1996**, *76*, 3830. (b) Thomas, L.; Lionti, F.; Ballou, R.; Gatteschi, D.; Sessoli, R.; Barbara, B. *Nature* **1996**, *383*, 145. (c) Tejada, J.; Ziolo, R. F.; Zhang, X. X. *Chem. Mater.* **1996**, *8*, 1784.
(6) (a) Eppley, H. J.; Tsai, H.-L.; de Vries N.; Folting K.; Christou, G.; Hendrickson, D. N. *J. Am. Chem. Soc.* **1995**, *117*, 301. (b) Aubin, S. M. J.; Spagna, S.; Eppley, H. J.; Sager, R. E.; Christou, G.; Hendrickson, D. N. *Chem. Commun.* **1998**, 803. (c) Aubin, S. M. J.; Sun, Z.; Pardi, L.; Krzystek, J.; Folting, K.; Brunel, L.-C.; Rheingold, A. L.; Christou, G.; Hendrickson, D. *Inorg. Chem.* **1999**, *38*, 5329. (d) Yoo, J.; Brechin, E. K.; Yamaguchi, A.; Rumberger, E. M.; Aubin, S. M. J.; Sun, Z.; Aromi, G. *Polyhedron* **2001**, *20*, 1479. (e) Kuroda-Sowa, T.; Nakano, M.; Christou, G.; Hendrickson, D. N. *Polyhedron* **2001**, *20*, 1537.
(7) (a) Soler, M.; Chandra, S. K.; Ruiz, D.; Davidson, E. R.; Hendrickson, D. N.; Christou, G. *Chem. Commun.* **2000**, 2417. (b) Soler, M.; Chandra, S. K.; Ruiz, D.; Huffman, J. C.; Hendrickson, D. N.; Christou, G. *Polyhedron* **2001**, *20*, 1279.
(8) (a) Boskovic, C.; Pink, M.; Huffman, J. C.; Hendrickson, D. N.; Christou, G. *J. Am. Chem. Soc.* **2001**, *123*, 9914. (b) Artus, P.; Boskovic, C.; Yoo, J.; Streib, W. E.; Brunel, L.-C.; Hendrickson, D. N.; Christou, G. *Inorg. Chem.* **2001**, *40*, 4199.

$(tacn)_6]^{8+}$ salts (where tacn is 1,4,7-triazacyclononane),[12] $[Fe_4(OMe)_6(dpm)_6]$ (dpm is the anion of dipivaloylmethane),[13] and $[V_4O_2(O_2CR)_7(L)_2]z$ (L is 2,2′-bipyridine or the pyridine-2-carboxylate anion).[14]

In an effort to obtain new high-spin molecules and possibly SMMs, we have been continuing our investigation into the usefulness of the chelating ligand hmp^- and the related ligand hep^- [where hepH is 2-(hydroxyethyl)pyridine] in Mn chemistry. In addition to the tetranuclear SMM $[Mn_4Br_2(H_2O)_2(hmp)_6]^{2+}$, with a ground-state spin of $S = 9$, we have previously reported several other Mn compounds incorporating hmp^-: $[Mn_4(O_2CR)_7(hmp)_2]^-$, $[Mn_{10}O_4(OH)_2(O_2CR)_8(hmp)_8]^{4+}$, and $[Mn_7(OH)_3Cl_3(hmp)_9]^{2+}$.[15−17] The last of these was found to have a spin ground state of ≥10; however, it proved to not be a SMM, presumably due to a relatively small magnetoanisotropy.

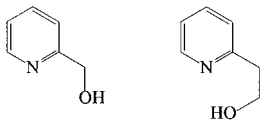

hmpH hepH

A synthetic methodology that has proved extremely useful in the past to access polynuclear Mn complexes is the reaction of a potential chelating ligand with a Mn carboxylate complex that does not already incorporate a chelating ligand. The trinuclear complexes of general formula $[Mn_3O(O_2CR)_6(L)_3]^{n+}$ ($n = 0, 1$; L = py, H_2O) have proved to be very useful starting materials for such reactions, affording complexes of nuclearity ranging from 2 to 10.[16,18] Herein we report the result of extending this synthetic methodology to reactions between $[Mn_8O_6Cl_6(O_2CPh)_7(H_2O)_2]^-$ and the potential chelating ligands hmpH and hepH. These have afforded the dodecanuclear title complexes $[Mn_{12}O_8Cl_4(O_2CPh)_8L_6]$ (L = hmp^-, hep^-). We describe the preparation, X-ray structure, and characterization of these complexes, including a detailed magnetochemical investigation of the solvation dependence of the properties of $[Mn_{12}O_8Cl_4(O_2CPh)_8(hmp)_6]$, which is a SMM. Aspects of this work have been communicated previously.[19]

Experimental Section

Syntheses. All manipulations were performed under aerobic conditions, using materials as received. $(NBu^n_4)[Mn_8O_6Cl_6(O_2CPh)_7(H_2O)_2]$ (**1**) was prepared as described.[20a]

$[Mn_{12}O_8Cl_4(O_2CPh)_8(hmp)_6]$ (2). hmpH (0.28 g, 2.6 mmol) was added to a stirred solution of $(NBu^n_4)[Mn_8O_6Cl_6(O_2CPh)_7(H_2O)_2]$ (1.22 g. 0.66 mmol) in MeCN (50 cm^3). After 2 days, a precipitate was isolated by filtration and washed with MeCN. The solid was recrystallized by layering two volumes of Et_2O onto a concentrated CH_2Cl_2 solution, which slowly gave brown crystals. The yield was 0.070 g (6%). A sample for crystallography was maintained in contact with the mother liquor to prevent the loss of interstitial solvent. Drying in air yielded a species that analyzed as $\mathbf{2}\cdot 0.7CH_2Cl_2$. Anal. calcd (found) for $C_{92.7}H_{77.4}N_6O_{30}Cl_{5.4}Mn_{12}$: C, 42.72 (42.44); H, 2.99 (3.19); N, 3.22 (3.23); Cl, 7.35 (7.30). Drying under vacuum leads to the unsolvated form. Anal. calcd (found) for $C_{92}H_{76}N_6O_{30}Cl_4Mn_{12}$: C, 43.39 (43.43); H, 3.01 (3.22); N, 3.30 (3.22); Cl, 5.57 (5.54). Selected IR data (KBr, cm^{-1}): 1601 (s), 1561 (s), 1543 (sh), 1521 (m), 1491 (w), 1485 (w), 1442 (m), 1306 (w), 1290 (m), 1254 (w), 1227 (w), 1175 (m), 1157 (m), 1104 (w), 1084 (sh), 1069 (m), 1050 (m), 1026 (w), 937 (w), 841 (w), 825 (w), 813 (w), 771 (m), 762 (m), 718 (s), 690 (m), 677 (m), 666 (m), 630 (s), 604 (m), 576 (m), 553 (m), 531 (m), 433 (w).

$[Mn_{12}O_8Cl_4(O_2CPh)_8(hep)_6]$ (3). hepH (0.27 g, 2.2 mmol) was added to a stirred solution of $(NBu^n_4)[Mn_8O_6Cl_6(O_2CPh)_7(H_2O)_2]$ (1.00 g, 0.54 mmol) in MeCN (40 cm^3). After 3 days, a precipitate was isolated by filtration and washed with MeCN. The solid was recrystallized by layering two volumes of Et_2O onto a concentrated CH_2Cl_2 solution, which slowly gave brown crystals. The yield was 0.14 g (15%). A sample for crystallography was maintained in contact with the mother liquor to prevent the loss of interstitial solvent. Drying under vacuum leads to the unsolvated form. Anal. calcd (found) for $C_{98}H_{88}N_6O_{30}Cl_4Mn_{12}$: C, 44.74 (44.23); H, 3.37 (3.30); N, 3.19 (3.09); Cl, 5.39 (5.33). Selected IR data (KBr, cm^{-1}): 1604 (s), 1568 (s), 1542 (m), 1490 (w), 1484 (w), 1444 (s), 1401 (s), 1311 (w), 1257 (w), 1220 (w), 1176 (w), 1152 (w), 1114 (m), 1071 (m), 1053 (m), 1036 (w), 1026 (m), 973 (w), 935 (w), 880 (w), 842 (w), 787 (w), 767 (w), 750 (w), 714 (s), 687 (m), 676 (m), 641 (s), 605 (s), 563 (m), 501 (m), 465 (m), 429 (m).

$[Mn_{12}O_8Br_4(O_2CPh)_8(hep)_6]$ (4). A 1.0 M solution of HBr in MeCN (0.16 cm^3, 0.16 mmol) was added to a solution of complex **3** (0.10 g, 0.038 mmol) in CH_2Cl_2 (10 cm^3). The reaction mixture was stirred overnight and then filtered through Celite. Et_2O (30 cm^3) was added dropwise to the vigorously stirred solution to produce a precipitate. The solid was collected by filtration and recrystallized by layering two volumes of Et_2O onto a concentrated CH_2Cl_2 solution, which slowly gave brown needles. The yield was 0.06 g (56%). A sample for crystallography was maintained in contact with the mother liquor to prevent the loss of interstitial solvent. After drying under vacuum, the sample analyzed for $\mathbf{4}\cdot 3H_2O$. Anal. calcd (found) for $C_{98}H_{94}N_6O_{33}Br_4Mn_{12}$: C, 41.12 (40.87); H, 3.31 (3.43); N, 2.94 (2.97); Br, 11.16 (9.96). Selected IR data (KBr, cm^{-1}): 1604 (s), 1567 (s), 1541 (m), 1485 (w), 1445 (s), 1401(s), 1310 (w), 1257 (w), 1218 (w), 1176 (w), 1159 (w), 1113 (m), 1077 (m), 1051 (m), 1026 (m), 973 (w), 939 (w), 878 (w), 842 (w), 787 (w), 767 (w), 754 (w), 716 (s), 688 (m), 675 (m), 641 (s), 607 (s), 563 (m), 500 (m), 464 (m), 435 (m).

(9) (a) Aubin, S. M. J.; Wemple, M. W.; Adams, D. M.; Tsai, H.-L.; Christou, G.; Hendrickson, D. N. *J. Am. Chem. Soc*. **1996**, *118*, 7746. (b) Wang, S.; Wemple, M. S.; Tsai, H.-L.; Folting, K.; Huffman, J. C.; Hagen, K. S.; Hendrickson, D. N.; Christou, G. *Inorg. Chem*. **2000**, *39*, 1501. (c) Aliaga, N.; Folting, K.; Hendrickson, D. N.; Christou, G. *Polyhedron* **2001**, *20*, 1273. (d) Mettes, F. L.; Aromi, G.; Luis, F.; Evangelisti, M.; Christou, G.; Hendrickson, D. N.; de Jongh, L. J. *Polyhedron* **2001**, *20*, 1459. (e) Andres, H.; Basler, R.; Gudel, H.-U.; Aromi, G.; Christou, G.; Buttner, H.; Ruffle, B. *J. Am. Chem. Soc*. **2000**, *122*, 12469.
(10) (a) Brechin, E. K.; Yoo, J.; Huffman, J. C.; Hendrickson, D. N.; Christou, G. *Chem. Commun.* **1999**, 783. (b) Yoo, J.; Brechin, E. K.; Yamaguchi, A.; Nakano, M.; Huffman, J. C.; Maniero, A. L.; Brunel, L.-C.; Awaga, K.; Ishimoto, H.; Christou, G.; Hendrickson, D. N. *Inorg. Chem*. **2000**, *39*, 3615.
(11) (a) Yoo, J.; Yamaguchi, A.; Nakano, M.; Krzystek, J.; Streib, W. E.; Brunel, L.-C.; Ishimoto, H.; Christou, G.; Hendrickson, D. N. *Inorg. Chem.* **2001**, *40*, 4604. (b) Bhattacharjee, A.; Miyazaki, Y.; Nakano, M.; Yoo, J.; Christou, G.; Hendrickson, D. N.; Sorai, M. *Polyhedron* **2001**, *20*, 1607.
(12) Sangregorio, C.; Ohm, T.; Paulsen, C.; Sessoli, R.; Gatteschi, D. *Phys. Rev. Lett.* **1997**, *78*, 4645.
(13) Barra, A.-L.; Caneschi, A.; Cornia, A.; Fabrizi de Biani, F.; Gatteschi, D.; Sangregorio, C.; Sessoli, R.; Sorace, L. *J. Am. Chem. Soc*. **1999**, *121*, 5302.
(14) Castro, S. L.; Sun, Z.; Grant, C. M.; Bollinger, J. C.; Hendrickson D. N.; Christou, G. *J. Am. Chem. Soc*. **1998**, *120*, 2997.
(15) Bouwman, E.; Bolcar, M. A.; Libby, E.; Huffman, J. C.; Folting, K.; Christou, G. *Inorg. Chem.* **1992**, *31*, 5185.
(16) Aromí, G.; Aubin, S. M. J.; Bolcar, M. A.; Christou, G.; Eppley, H. J.; Folting, K.; Hendrickson, D. N.; Huffman, J. C.; Squire, R. C.; Tsai, H.-L.; Wang, S.; Wemple, M. W. *Polyhedron* **1998**, *17*, 3005.
(17) Bolcar, M. A.; Aubin, S. M. J.; Folting, K.; Hendrickson, D. N.; Christou, G. *Chem. Commun.* **1997**, 1485.
(18) (a) Christou, G. *Acc. Chem. Res.* **1989**, *22*, 328. (b) Aromi, G.; Aubin, S. M. J.; Bolcar, M.; Christou, G.; Eppley, H. J.; Folting, K.; Hendrickson, D. N.; Huffman, J. C.; Squire, R. C.; Tsai, H.-L.; Wang, S.; Wemple, M. W. *Polyhedron* **1998**, *17*, 3005
(19) Boskovic, C.; Brechin, E. K.; Streib, W. E.; Folting, K.; Hendrickson, D. N.; Christou, G. *J. Chem. Soc., Chem. Commun.* **2001**, 467.
(20) (a) Tsai, H.-L.; Wang, S.; Folting, K.; Streib, W. E.; Hendrickson, D. N.; Christou, G. *J. Am. Chem. Soc.* **1995**, *117*, 2503. (b) Chisholm, M. H.; Folting, K.; Huffman, J. C.; Kirkpatrick, C. C. *Inorg. Chem.* **1984**, *23*, 1021.

Table 1. Crystallographic Data for Complexes **2**·$2Et_2O$·$4CH_2Cl_2$, **3**·$7CH_2Cl_2$, and **4**·$2Et_2O$·$1.4CH_2Cl_2$

	2	**3**	**4**
formula[a]	$C_{104}H_{104}N_6O_{32}Cl_{12}Mn_{12}$	$C_{105}H_{102}N_6O_{30}Cl_{18}Mn_{12}$	$C_{107.4}H_{110.8}N_6O_{32}Cl_{2.8}Br_4Mn_{12}$
fw, g mol^{-1}	3034.68	3225.39	3075.82
space group	$P\bar{1}$	$C2/c$	$I4_1/a$
a, Å	14.260(1)	36.774(3)	41.1530(6)
b, Å	14.824(1)	14.930(1)	41.1530(6)
c, Å	15.793(1)	27.037(3)	14.3127(3)
α, deg	94.558(2)		
β, deg	92.773(2)	121.884(3)	
γ, deg	114.916(2)		
V, $Å^3$	3006	12 604	24 240
Z	1	4	8
T, °C	−160	−168	−161
λ, Å[b]	0.71073	0.71069	0.71073
ρ_{calc}, g cm^{-3}	1.676	1.700	1.685
μ, cm^{-1}	15.56	16.12	26.63
obsd data ($I > 2\sigma I$)	9258	7908	9560
R (R_w), %[c,d]	6.23 (6.98)	3.53 (3.79)	5.10 (13.53)

[a] Including solvate molecules. [b] Graphite monochromator. [c] $R = 100\Sigma||F_o| - |F_c||/\Sigma|F_o|$. [d] $R_w = 100[\Sigma w(|F_o| - |F_c|)^2/\Sigma w|F_o|^2]^{1/2}$, where $w = 1/\sigma^2(|F_o|)$.

X-ray Crystallography. Data were collected on a Bruker platform goniometer equipped with a Smart 6000 CCD detector (**2**·$2Et_2O$·$4CH_2Cl_2$ and **4**·$2Et_2O$·$1.4CH_2Cl_2$) or on a Picker four-circle diffractometer at (**3**·$7CH_2Cl_2$). Details of the diffractometry, low-temperature facilities, and computational procedures employed by the Molecular Structure Center are available elsewhere.[20b] Data collection and structure solution details are listed in Table 1. For all complexes, data were corrected for absorption effects and equivalent data were averaged. The structures of **2**·$2Et_2O$·$4CH_2Cl_2$ and **4**·$2Et_2O$·$1.4CH_2Cl_2$ were solved by direct methods (SHELXTL) and standard Fourier techniques. The structure of **3**·$7CH_2Cl_2$ was solved by a combination of direct and Patterson methods (DIRDIF-96) and standard Fourier techniques. All structures were refined by full-matrix least-squares methods.

For complex **2**·$2Et_2O$·$4CH_2Cl_2$, a systematic search of a limited hemisphere of reciprocal space revealed a set of reflections with no symmetry and no systematic absences. An initial choice of the centrosymmetric space group $P\bar{1}$ was subsequently confirmed by the successful solution of the structure. The asymmetric unit was found to contain half of the molecule of interest, two molecules of CH_2Cl_2, and one molecule of slightly disordered Et_2O solvent. Most of the atoms in the molecule were located in the initial best solution. In the final cycles of refinement the non-hydrogen atoms were refined by use of anisotropic thermal parameters, with the exception of C(83) and C(84), the half-weight atoms on one arm of the Et_2O, which were kept isotropic. Many of the hydrogen atoms were visible in a difference Fourier map following initial refinement cycles. Hydrogen atoms were then introduced in fixed calculated positions. The final difference Fourier map was essentially featureless, the largest peak being 1.79 e $Å^{-3}$ located 1.7 Å from Cl(77). The deepest hole was −1.65 e $Å^{-3}$.

For complex **3**·$7CH_2Cl_2$ a preliminary search for peaks and analysis revealed a *C*-centered monoclinic cell. Following intensity data collection, the additional condition $l = 2n$ for $h0l$ limited the space group to *Cc* or *C*2/*c*. Subsequent solution and refinement of the structure confirmed the choice of *C*2/*c*. The asymmetric unit was found to contain half of the molecule of interest, in addition to 3.5 molecules of CH_2Cl_2. All non-hydrogen atoms were readily located and refined anisotropically. Hydrogen atoms were included in fixed calculated positions in the final cycles of refinement. The final difference Fourier map was essentially featureless, the largest peak being 0.264 e $Å^{-3}$ and the deepest hole −0.260 e $Å^{-3}$.

For complex **4**·$2Et_2O$·$1.4CH_2Cl_2$, a systematic search of a limited hemisphere of reciprocal space revealed tetragonal symmetry and systematic absences corresponding uniquely to the centrosymmetric space group $I4_1/a$. Subsequent solution and refinement of the structure confirmed this choice. The asymmetric unit was found to contain half of the molecule of interest in addition to some disordered solvent. A partially occupied (about 70% present) CH_2Cl_2 molecule was resolved, but electron density peaks corresponding to another small molecule, probably a highly disordered Et_2O, could not be represented by a chemically reasonable model. The electron density corresponding to the disordered molecule was modeled by several partially occupied carbon atoms [C(79)−C(89)]. Except for these, all non-hydrogen atoms were refined anisotropically. Hydrogen atoms were placed in calculated positions and refined with the use of a riding model. The final difference Fourier map was essentially featureless, the largest peak being 1.10 e $Å^{-3}$ near the disordered solvent.

Other Measurements. Infrared spectra (KBr disk) were recorded on a Nicolet model 510P spectrophotometer. Elemental analyses were performed by Atlantic Microlab, Inc., Norcross, GA. Variable-temperature magnetic susceptibility measurements employed a Quantum Design MPMS-XL SQUID susceptometer equipped with a 70 kG (7 T) magnet. Data were collected on powdered samples or intact crystals freshly removed from the mother liquor; they were restrained in eicosane to prevent torquing and to retard solvent loss from the intact crystals. For solution measurements, data were collected on frozen, saturated dimethylformamide (DMF) solutions (∼1 mg in 0.3 cm^3). Pascal's constants were used to estimate the diamagnetic correction for each complex, which was subtracted from the experimental susceptibility to give the molar magnetic susceptibility (χ_M).

Results and Discussion

Syntheses. Treatment of an MeCN solution of $(NBu^n_4)[Mn_8O_6Cl_6(O_2CPh)_7(H_2O)_2]$ (**1**) with 4 equiv of HL (L = hmp^-, hep^-) leads to the formation of a precipitate after several days. Extraction of the soluble component of this material into CH_2Cl_2 and diffusion of Et_2O into the resulting solution leads to the formation of crystalline $[Mn_{12}O_8Cl_4(O_2CPh)_8(L)_6]$, where L = hmp^- (**2**) or hep^- (**3**). For both compounds the final yield is low, 6% and 15%, respectively; nevertheless, the preparations are reproducible. As is usually the case for such reactions, several species in equilibrium are likely present in solution, and the low solubility of one of them is undoubtedly the reason a pure product can be obtained. IR spectroscopy suggests that Mn oxides comprise the bulk of the material that precipitates from solution. The transformation of **1** into **2** or **3** is summarized in eq 1:

$$3[Mn_8O_6Cl_6(O_2CPh)_7(H_2O)_2]^- + 12HL + 4e^- \rightarrow 2[Mn_{12}O_8Cl_4(O_2CPh)_8(L)_6] + 8H_2O + 10Cl^- + 5PhCO_2^- + 8H^+ \quad (1)$$

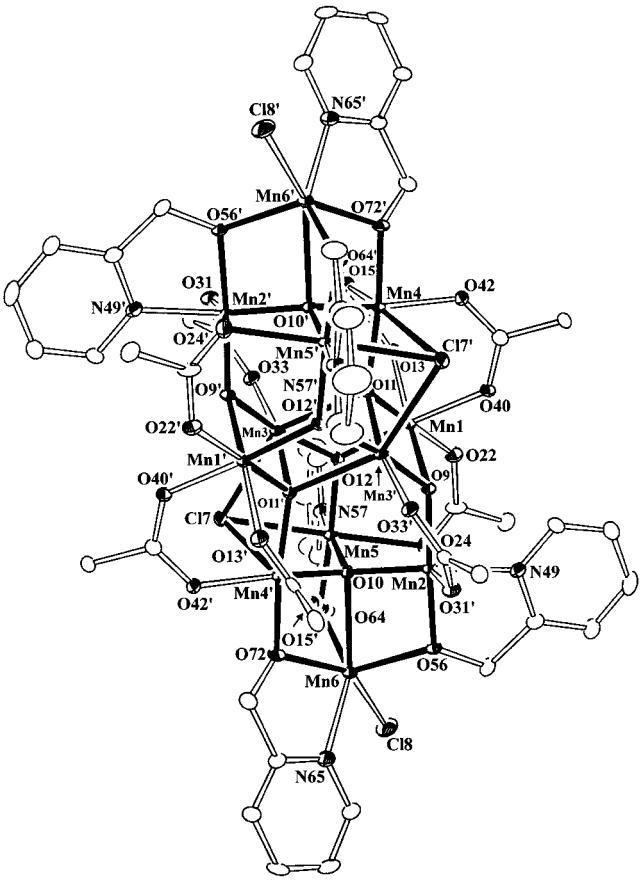

Figure 1. ORTEP representation of complex **2** at the 50% probability level. For clarity, only the *ipso* carbon of each phenyl ring is included.

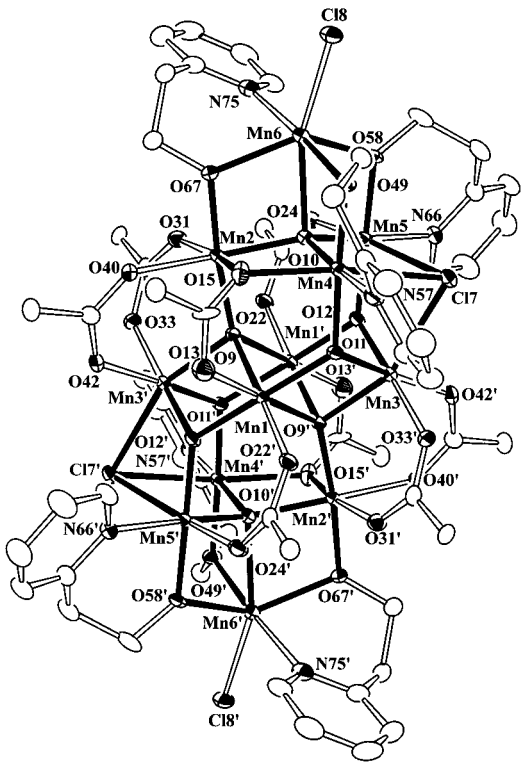

Figure 2. ORTEP representation of complex **3** at the 50% probability level. For clarity, only the *ipso* carbon of each phenyl ring is included.

Table 2. Selected Structural Parameters for Complexes **2** and **3**

parameter[a]	**2**	**3**
$Mn^{II}\cdots Mn^{III}$	3.291(1)−3.372(1)	3.206(1)−3.279(1)
$Mn^{III}\cdots Mn^{III}$	3.012(1)−3.758(1)	2.977(1)−3.708(1)
$Mn^{II}-Cl_t$	2.469(1)	2.424(1)
$Mn^{III}-Cl_b$	2.618(1)−2.847(2)	2.628(1)−2.790(1)
$Mn^{II}-O_o$	2.455(3)	2.261(3)
$Mn^{III}-O_o$	1.851(3)−2.329(3)	1.852(3)−2.311(3)

[a] b = bridging, t = terminal, o = oxide.

The products **2** and **3** are mixed-valence $2Mn^{II},10Mn^{III}$, whereas **1** is $8Mn^{III}$; thus, formation of **2** and **3** appears to involve the reduction of **1**, presumably accompanied by oxidation of hmpH/hepH as confirmed in related work.[21] Analogous redox chemistry has also been observed previously with these and similar ligands in the formation of tetranuclear and octadecanuclear Mn clusters.[10,11,22] Hence a complex mechanism involving redox chemistry, fragmentation, and structural rearrangement must be invoked to explain the formation of **2** and **3**.

Compound **3** may also be isolated in similar yield following reaction of **1** with 8 equiv of hepH. However, the use of greater than 4 equiv of hmpH seems to inhibit the formation of **2**. In addition, while **3** appears to be stable in solution and is spectroscopically identical upon repeated recrystallizations, **2** is not. Infrared spectroscopy and elemental analysis indicate that repeated recrystallization of **2** leads to the formation of a new species that we are currently attempting to characterize.

Reaction of a CH_2Cl_2 solution of **3** with 4 equiv of a 1 M solution of aqueous HBr in MeCN leads to isolation of crystalline $[Mn_{12}O_8Br_4(O_2CPh)_8(hep)_6]$ (**4**) in good yield (56%). Such a metathesis reaction (eq 2)

$$[Mn_{12}O_8Cl_4(O_2CPh)_8(hep)_6] + 4HBr \rightarrow [Mn_{12}O_8Br_4(O_2CPh)_8(hep)_6] + 4HCl \quad (2)$$

is apparently more favorable than protonation of either the hep^- or $PhCO_2^-$ ligands. Compound **4** is spectroscopically extremely similar to **3** and, like **3**, appears to be stable in solution.

Description of Structures. Labeled ORTEP plots of **2** and **3** are shown in Figures 1 and 2, respectively. A comparison of selected metric parameters is provided in Table 2. An ORTEP plot for **4** and tables of pertinent metric parameters for complexes **2**−**4** are available in Supporting Information, together with stereoviews of complexes **2** and **3**. Complex **2**·$2Et_2O$·$4CH_2Cl_2$ crystallizes in the triclinic space group $P\bar{1}$, complex **3**·$7CH_2Cl_2$ crystallizes in the monoclinic space group $C2/c$, and complex **4**·$2Et_2O$·$1.4CH_2Cl_2$ crystallizes in the tetragonal space group $I4_1/a$. Disregarding the difference in chelating ligand, complexes **2** and **3** can be considered as structural isomers, while complex **4** is essentially isostructural with **3**. Thus, the general structural features will be discussed first, followed by a comparison focusing on structural differences.

The clusters consist of an $[Mn^{III}_{10}Mn^{II}_2(\mu_4\text{-}O)_4(\mu_3\text{-}O)_4(\mu_2\text{-}O)_8(\mu_3\text{-}X)_2]$ core (Figure 3), and peripheral ligation is provided by six hmp^- (**2**) or hep^- (**3** and **4**) ligands, eight $PhCO_2^-$ ligands, and two terminal X^- ligands (Cl^- for **2** and **3**, Br^- for **4**). The molecules all lie on an inversion center with C_i point symmetry.

(21) Boskovic, C.; Folting, K.; Huffman, J. C.; Wernsdorfer, W.; Hendrickson, D. N.; Christou, G. *Inorg. Chem.*, submitted for publication.
(22) Brechin, E. K.; Yoo, J.; Concolino, T. E.; Rheingold, A. L.; Hendrickson, D. N. Christou, G. Manuscript in preparation.

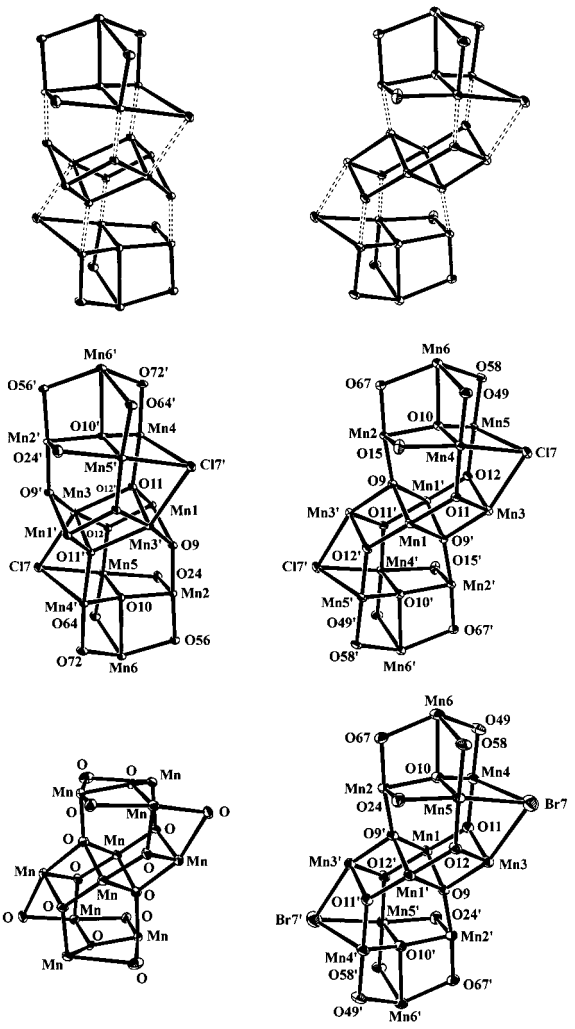

Figure 3. Construction of the cores from two Mn_4O_5Cl end units and one Mn_4O_6 middle unit (top) and the cores of complexes **2**, **3**, **4**, and **5** (bottom, clockwise from top left).

For the sake of brevity, references to specific atoms in the following discussion implicitly include their symmetry-related partners.

Bond valence sums indicate that the two Mn^{II} atoms of each cluster are those at either end, Mn(6). Each Mn atom is in a distorted octahedral environment, with the Mn^{II} atoms displaying the most severe distortions (vide infra). The eight μ_3- and μ_4-O atoms of the core are provided by O^{2-} ions, while the eight μ_2-O atoms are provided by the six hmp^-/hep^- ligands and by two of the $PhCO_2^-$ groups. The core can be considered to comprise three pairs of face-sharing cuboids (Figure 3) i.e., incomplete face-sharing double cubanes. The two Mn_4O_5Cl "end" units are each deficient of two vertexes on the same edge of the unit, and the Mn_4O_6 "middle" unit is deficient of two vertexes that are diagonally opposed through the body of the unit. In fact, if the μ_2-O atoms from the $PhCO_2^-$ ligands [**2** and **4**, O(24); **3**, O(15)] are disregarded, the core possesses an approximate mirror plane passing through Mn(2), Mn(3), Mn-(6), O(9), O(10), and O(56) (**2**) or O(67) (**3** and **4**).

Of the peripheral ligands, all 12 $PhCO_2^-$ groups bind in a syn,syn manner, 10 of them in the usual μ_2 fashion and two in the rarer μ_3 mode, with one O atom bridging two Mn atoms and the other O atom terminal to a third Mn atom. All six of the hmp^- (**2**) or hep^- (**3** and **4**) ligands bind in a μ_2 fashion, chelating one Mn atom and simultaneously bridging it to another through the O atom. For each cluster, two of the hmp^- (or hep^-) ligands chelate the Mn^{II} atoms and bridge them to a Mn^{III} atom from the end unit, while the remaining four ligands chelate the other Mn^{III} atoms of the end units and bridge them to the Mn^{II} atom. The eight $PhCO_2^-$ groups serve to bridge Mn atoms from the middle unit with those from the end units.

The ten Mn^{III} atoms in each cluster display a Jahn−Teller (JT) distortion, as expected for high-spin Mn^{III} (d^4) in near-octahedral geometry. For the six Mn^{III} atoms [Mn(3), Mn(4), and Mn(5)] bound to the μ_3-X, the axially elongated sites are all occupied by the Cl atom and the trans O atom (oxo or $PhCO_2^-$). For the two Mn^{III} atoms of the end units that are not bound to the μ_3-X atom [Mn(2)], the axially elongated sites are occupied by the μ_2-O atoms of the μ_3-$PhCO_2^-$ ligands [**2** and **4**, O(24); **3**, O(15)] and the trans O atoms ($PhCO_2^-$). Thus, the μ_2-O atoms of the μ_3-$PhCO_2^-$ ligands lie on the JT axes of both of the Mn atoms to which they are bound. For the remaining Mn^{III} atoms of the middle unit [Mn(1)], the axially elongated sites are occupied by the bridging O atoms (oxo) [**2**, O(11); **3** and **4**, O(9)] and the O atoms ($PhCO_2^-$) trans to them. As a result of the JT elongated bonds, all of the Mn···Mn separations are ca. 3.0 Å or greater.

Comparison of the Structures of 2 and 3. Disregarding the difference in chelating ligand, compounds **2** and **3** possess the same formula and display similar connectivities. The difference in their cores arises from the way in which the three pairs of face-shared double cuboids are linked together (Figure 3). The two Mn_4O_5Cl end units effectively sandwich the Mn_4O_6 middle unit in both compounds. However, the orientation of the middle units differs by a 120° rotation around an axis passing through the center of the unit and perpendicular to the planes defined by Mn(1) and Mn(3). Consequently, the Mn atoms of the middle unit that bind to the μ_3-Cl ligands, Mn(3), lie along the edges of the middle unit for **2** and on a corner of the middle unit for **3**. The differences in bond lengths between equivalent bonds in the cores of the two compounds are generally less than 0.1 Å. The two bond distances that display a greater disparity are Mn(6)···O(10) (**2**, 2.46 Å; **3**, 2.26 Å) and Mn(2)···O(24) (**2**, 2.64 Å) vs Mn(2)···O(15) (**3**, 2.36 Å). In addition, the corresponding angles between the two species are of comparable magnitude.

The differences between the cores of **2** and **3** lead to a number of differences in their peripheral ligation. In both cases, the chelating ligands (hmp^- for **2** and hep^- for **3**) chelate Mn(6) and two of the three Mn^{III} atoms of the end unit. In the case of **2**, Mn(2) and Mn(5) are chelated by hmp^- and the ligands are symmetrically disposed on either side of the μ_3-$PhCO_2^-$ ligand. However, for **3** these are Mn(4) and Mn(5), and instead the hep^- ligands are symmetrically disposed on either side of the μ_3-Cl ligand. Associated with the differing chelate ring sizes, the "bite angles" also vary between the species, with hmp^- angles of 81.2°, 82.7°, and 72.4° and hep^- angles of 91.8°, 91.7°, and 77.7°. In addition, the five-member chelate rings of **2** are approximately planar, in contrast to the distinctly nonplanar six-member chelate rings in **3**.

The arrangement of the $PhCO_2^-$ ligands also differs between the two compounds. One consequence is that in **2** only four of the eight $PhCO_2^-$ phenyl rings participate in intramolecular

π-stacking interactions (average separation of 3.9 Å), whereas in **3** all eight of the $PhCO_2^-$ phenyl rings participate in intramolecular π-stacking interactions in four pairs (average separations of 3.8 and 3.9 Å).

The JT axes for the atoms Mn(2), Mn(3), Mn(4), and Mn(5) are consistent between **2** and **3**. However, different JT axes are observed for the Mn atoms on the edge of the Mn_4O_5Cl middle unit [Mn(1)]. As a result, in **2** the μ_4-O (oxo) atoms [O(11)] lie on the JT axis of a single Mn atom [Mn(1)], while the equivalent atoms in **3**, [O(9)], lie on the JT axes of two Mn atoms [Mn(1) and Mn(3)].

In both **2** and **3**, the geometry at Mn^{II} atom Mn(6) is extremely distorted from octahedral; however, in **2** the distortion is so severe that the coordination is better described as trigonal prismatic. The trigonal faces comprise atoms Cl(8), O(56), N(65) and O(64), O(10), O(72), and the twist angles [Cl(8)−Ct−Ct′−O(64), O(56)−Ct−Ct′−O(10), and N(65)−Ct−Ct′−O(72), where Ct and Ct′ are the centroids of each triangular face] are 8.5°, 5.0°, and 9.8°. These angles are far from the ideal angles of 60° for true octahedral geometry and closer to the trigonal prismatic ideal of 0°. In contrast for **3**, the equivalent angles for Cl(8)−Ct−Ct′−O(10), O(67)−Ct−Ct′−O(49), and N(75)−Ct−Ct′−O(58) are 56.3°, 27.7°, and 42.1°, which are consistent with distorted octahedral geometry. The difference between the two compounds is primarily due to the differing bite angles of the chelate ligands combined with the large size of the Mn^{II} ion;[23] the bite angle of the hmp^- ligand is too small to allow a more octahedral geometry at Mn^{II}. Trigonal prismatic geometry for Mn^{II} is uncommon but has previously been reported for mononuclear and dinuclear compounds.[24]

A consideration of intermolecular interactions is relevant to the discussion that follows of the magnetochemical properties of these species. Complex **2** appears to possess a number of weak intermolecular interactions in the form of hydrogen bonds and intermolecular π-stacking interactions. The hydrogen bonds involve C−H bonds and are of the C−H···O and C−H···Cl variety,[25] involving O^{2-} and Cl atoms, and C−H units of both the Mn_{12} complex and the CH_2Cl_2 interstitial solvent molecules. There are 11 C−H···Cl and two C−H···O interactions (diagrams available in Supporting Information) with C···Cl and C···O distances of 3.5−3.8 and ∼3.2 Å, respectively, and C−H···Cl and C−H···O angles of >115°, and 153.3 and 122.0°, respectively; these values are typical of these types of hydrogen-bonding contacts. The interatomic separations are listed in Table 3. In addition, there are two types of weak intermolecular π-stacking interactions, one between hmp^- pyridine rings [N(65)−C(70)] on adjacent molecules, and the other between benzoate phenyl rings [C(16)−C(21)] on adjacent molecules. These have average separations of the aromatic rings of 4.3 and 4.7 Å, respectively, larger than the 3.9 Å for the intramolecular interactions and the separations usually taken as π-stacking interactions; nevertheless these constitute weak interactions. Complex **3** also appears to possess weak intermolecular hydrogen bonds, involving the atoms of the complex and of the CH_2Cl_2 molecules. The X-ray structure reveals a single C−H···O hydrogen bond involving C(84)−H(50)···O(42), with a C···O distance of ∼3.5 Å and a C−H···O angle of 131.1°. In addition, there are 20 possible C−H···Cl interactions with C···Cl distances of 3.5−3.8 Å and C−H···Cl angles of >115°. However, no intermolecular π-stacking interactions are observed for **3**, which is consistent with the fact that all eight of the $PhCO_2^-$ ligands are involved in intramolecular π-stacking interactions and that the pyridine ligands of the hep^- ligands appear to "protrude" less from the bulk of the complex than those of the hmp^- ligands of complex **2**. Complexes **3** and **4** are effectively isostructural, with the only significant differences being due to the different sizes of Cl and Br atoms.

Table 3. Possible Hydrogen-Bonding Interactions for Complex **2**·$2Et_2O$·$4CH_2Cl_2$

atoms[a]	X···H–C (deg)	X···C (Å)
O(13)···H(39)−C(73)	153.3	3.205
O(64)···H(35′)−C(68′)	122.0	3.196
Cl(7)···H(19)−C(47)	133.4	3.674
Cl(7)···H(18)−C(46)	121.0	3.769
Cl(7)···H(35′)−C(68′)	128.1	3.618
Cl(8)···H(12)−C(36)	121.8	3.618
Cl(8)···H(42)−C(76)	137.8	3.686
Cl(75)···H(10)−C(30)	130.3	3.646
Cl(75)···H(14′)−C(38′)	146.9	3.639
Cl(75)···H(28′)−C(59′)	129.3	3.581
Cl(77)···H(30′)−C(61′)	139.3	3.708
Cl(77)···H(31)−C(63)	118.9	3.715
Cl(78)···H(32)−C(63)	142.4	3.745

[a] Cl(75), Cl(77), and Cl(78) are CH_2Cl_2 atoms.

Complexes **2**−**4** are a new structural type, with the other known family of Mn_{12} clusters $[Mn_{12}O_{12}(O_2CR)_{16}(H_2O)_x]$ (x = 3 or 4) possessing a distinctly different structure.[2,3,26] However, part of the core of **3** (and **4**) has been observed previously in $[Mn_{10}O_8(O_2CPh)_6(pic)_8]$ (**5**), where pic^- is the anion of 2-picolinic acid.[27] The core of **3** can be obtained from the $[Mn^{III}_{10}(\mu_4\text{-}O)_2(\mu_3\text{-}O)_6(\mu_2\text{-}O)_6]^{2+}$ core of **5** by the removal of four μ_2-O atoms and the addition of two Mn^{II} atoms [Mn(6)], two μ_3-Cl atoms [Cl(7)] and six μ_2-O atoms [O(49), O(58) and O(67)] (Figure 3). The bond lengths and bond angles of the conserved moiety are extremely similar for **5** and **3**. However, there is considerable difference in the arrangement of the peripheral ligands, despite the incorporation of bridging $PhCO_2^-$ ligands in both compounds and the similarity between the chelating ligands, pic^- and hmp^-. In contrast to **3**, all of the $PhCO_2^-$ ligands in **5** bind in the μ_3 mode and no π-stacking interactions are possible between the phenyl rings. In addition, the chelating ligands in **5** do not also serve in a bridging capacity.

Different Forms of Complex 2. During the course of study of complex **2** it became apparent that there are at least four different forms of this material, with the magnetic behavior of all of these species being reported herein. There is the solvated form characterized in the X-ray structure, **2**·$2Et_2O$·$4CH_2Cl_2$. When allowed to stand in air, this form rapidly loses solvent molecules, accompanied by loss of crystallinity to yield a powder. After drying in air, this partially solvated material analyzed as **2**·$0.7CH_2Cl_2$. Complete removal of the solvent is

(23) Weast, R. C., Ed. *CRC Handbook of Chemistry and Physics*, 64th ed.; CRC Press Inc.: Boca Raton, FL, 1983; p F170.
(24) (a) Belal, A. A.; Chaudhuri, P.; Fallis, I.; Farrugia, L.; Hartung, R.; Macdonald, N. M.; Nuber, B.; Peacock, R. D.; Weiss, J.; Wieghardt, K. *Inorg. Chem.* **1991**, *30*, 4397. (b) Arulsamy, N.; Glerup, J.; Hodgson, D. J. *Inorg. Chem.* **1994**, *33*, 3045. (c) Brudenall, S. J.; Spiccia, L.; Bond, A. M.; Fallon, G. D.; Hockless, D. C. R.; Laxarev, G.; Mahon, P. J.; Tiekink, E. R. T. *Inorg. Chem.* **2000**, *39*, 881.
(25) (a) Taylor, R.; Kennard, O. *J. Am. Chem. Soc.* **1982**, *104*, 5063. (b) Desiraju, G. R. *Acc. Chem. Res.* **1996**, *29*, 441.
(26) Lis, T. *Acta Crystallogr.* **1980**, *B36*, 2042.
(27) Eppley, H. J.; Aubin, S. M. J.; Streib, W. E.; Bollinger, J. C.; Hendrickson, D. N.; Christou, G. *Inorg. Chem.* **1997**, *36*, 109.

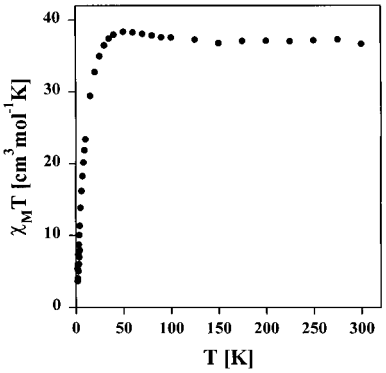

Figure 4. Plot of $\chi_M T$ vs temperature for a powder sample of unsolvated complex **2** in eicosane. χ_M is the dc magnetic susceptibility measured in a 10 kG field.

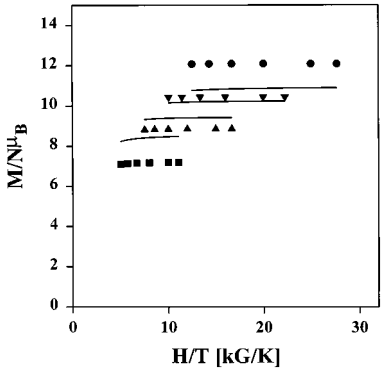

Figure 5. Plot of $M/N\mu_B$ vs H/T for a powder sample of unsolvated complex **2** in eicosane at 20 (■), 30 (▲), 40 (▼), and 50 (●) kG. The solid lines are fits to $S = 7$ by the appropriate method; see the text for other fitting parameters and those for the $S = 6$ fit.

possible by drying in a vacuum, to afford the unsolvated species **2**. Note that allowing this material to stand in air does not lead to hydration, as has sometimes been observed for similar complexes.[10b,27] Finally, dissolution in DMF and freezing of the solution affords a sample whereby the individual molecules are well separated and can be considered to be infinitely solvated.

Magnetochemistry of Complex 2. Variable-temperature dc susceptibility measurements were performed on unsolvated **2**, restrained in eicosane to prevent torquing, in a 10 kG field in the range 1.8−300 K (Figure 4). The $\chi_M T$ value of 36.6 cm^3 mol^{-1} K at 300 K remains approximately constant as the temperature is decreased until ∼100 K, when it begins to increase to a maximum value of 38.3 cm^3 mol^{-1} K at 50 K before rapidly decreasing to 5.3 cm^3 mol^{-1} K at 1.8 K. The spin-only ($g = 2$) value for a unit composed of noninteracting $Mn^{II}_2Mn^{III}_{10}$ ions is 38.8 cm^3 mol^{-1} K. Hence, the molecule appears to have a high-spin ground state, with the low-temperature decrease assigned to some combination of zero-field splitting (ZFS), Zeeman effects, and antiferromagnetic intermolecular interactions.

Complex **2** contains ten Mn^{III} and two Mn^{II} centers. The total spin (S_T) values of the different resultant states range from 0 to 25. This large number of spin states makes it effectively impossible to evaluate the exchange parameters that characterize the pairwise exchange interactions in the spin Hamiltonian. In addition, owing to the size and low symmetry of the molecule, it is not possible to use the Kambe approach to derive a theoretical equation to fit the $\chi_M T$ vs T data.[28]

To determine the spin ground state, magnetization data were collected in the ranges 20−50 kG and 1.8−4.0 K, and plotted as reduced magnetization ($M/N\mu_B$) vs H/T (Figure 5), where N is Avogadro's number and μ_B is the Bohr magneton. For a system occupying only the ground state and experiencing no zero-field splitting (ZFS), the various isofield lines would be superimposed and $M/N\mu_B$ would saturate at a value of gS. The nonsuperposition of the isofield lines clearly indicates ZFS. Attempts to fit the data by the methods described elsewhere,[11a] involving a full diagonalization of the spin Hamiltonian matrix including axial ZFS and Zeeman interactions and assuming that only the ground state is populated, produced best fits of $S = 6$, $g = 2.09$, $D \sim -0.8$ (−1.1 K) cm^{-1} and $S = 7$, $g = 1.79$, $D \sim -0.6$ cm^{-1} (−0.8 K), where D is the axial ZFS parameter. These fits were of comparable quality but poorer than those normally obtained. This is a common problem in higher nuclearity Mn_x systems and is assignable to the population of relatively low-lying excited states,[22,29] particularly when Mn^{II} ions are present, since these always give weak exchange interactions. We conclude that the molecule has $S = 6$ or 7 but are unable to accurately determine the value of D from these data.

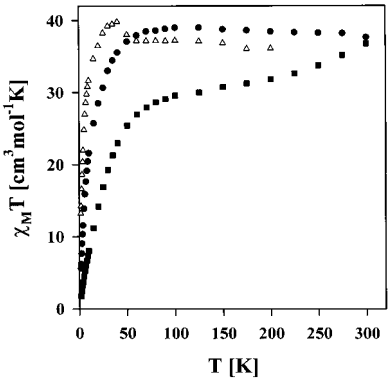

Figure 6. Plot of $\chi_M T$ vs temperature for a powder sample of **2**·0.7CH_2Cl_2 in eicosane (●), intact crystals of **2**·2Et_2O·4CH_2Cl_2 in eicosane (■), and a frozen solution of **2** in DMF (△). χ_M is the dc magnetic susceptibility measured in a 10 kG field.

To investigate the effect of solvation on the magnetic behavior of complex **2**, variable-temperature dc susceptibility measurements were performed in a 10 kG field in the range 1.8−300 K on (i) a powder sample of **2**·0.7CH_2Cl_2, restrained in eicosane to prevent torquing; (ii) a frozen solution of **2** in DMF (∼1 mg in 0.3 cm^3), and (iii) a collection of intact crystals of **2**·2Et_2O·4CH_2Cl_2, removed from the mother liquor and immediately immersed in liquid eicosane (to retard solvent loss as well as to prevent torquing) before being placed directly in the SQUID instrument. Significantly different behavior is observed for the three samples (Figure 6). The $\chi_M T$ profile for complex **2**·0.7CH_2Cl_2 is quite similar to that of the unsolvated form of **2**, with a $\chi_M T$ of 37.6 cm^3 mol^{-1} K at 300 K increasing gradually to a value of 39.0 cm^3 mol^{-1} K as the temperature is decreased to 125 K and then rapidly decreasing to 5.6 cm^3 mol^{-1} K at 1.8 K. The behavior of the frozen solution of complex **2** in DMF is also somewhat similar to that of unsolvated **2**. In this case the $\chi_M T$ value increases gradually from a value of 36.0

(28) Kambe, K. J. *Phys. Soc. Jpn.* **1950**, *48*, 15.

(29) Soler, M.; Rumberger, E.; Folting, K.; Hendrickson, D. N.; Christou, G. *Polyhedron* **2001**, *20*, 1365.

$cm^3\ mol^{-1}$ K at 200 K until ~50 K, where it increases sharply to a maximum value of 39.8 $cm^3\ mol^{-1}$ K at 40 K, before rapidly decreasing to 13.2 $cm^3\ mol^{-1}$ K at 1.8 K. In contrast, the behavior of **2**·$2Et_2O$·$4CH_2Cl_2$ is somewhat different, with $\chi_M T$ decreasing gradually from a value of 36.7 $cm^3\ mol^{-1}$ K at 300 K, almost leveling off at a value of ~30 $cm^3\ mol^{-1}$ K between 200 and 100 K, and then rapidly decreasing to a value of 1.8 $cm^3\ mol^{-1}$ K at 1.8 K.

The $\chi_M T$ vs temperature behavior for unsolvated **2**, **2**·$0.7CH_2Cl_2$, and the frozen DMF solution of **2** are reasonably consistent, each displaying an increase in the $\chi_M T$ value as the temperature is decreased from 300 to ~40 K. This is most pronounced for the frozen solution, despite the fact that this plot is the noisiest owing to the relatively small amount of material in solution and the relatively large background that must be subtracted. As the temperature is further decreased, a sharp drop is observed in the value of $\chi_M T$. The behavior of the intact crystals of **2**·$2Et_2O$·$4CH_2Cl_2$ in eicosane is somewhat different, with the value of $\chi_M T$ decreasing gradually as the temperature is decreased from 300 K, almost leveling off between 200 and 100 K, and then rapidly decreasing as the temperature is further lowered. This is suggestive of two distinct processes, with the effect of antiferromagnetic intramolecular exchange interactions observed at relatively high temperatures, which are then dominated by the effect of some combination of ZFS, Zeeman effects, and antiferromagnetic intermolecular interactions, causing the rapid decrease in $\chi_M T$ as the temperature approaches 0 K. The origin of the different behavior between the unsolvated, slightly solvated, and frozen solution species on one hand and the fully solvated crystals on the other is uncertain. However, it is clearly related to the presence of solvate molecules. Note that the low-temperature (<40 K) decrease in $\chi_M T$ is greatest for **2**·$2Et_2O$·$4CH_2Cl_2$ and smallest for the frozen solution of **2**, suggesting that antiferromagnetic intermolecular interactions may contribute significantly to the behavior observed in this temperature regime. Intermolecular interactions will be the least in solution, where the molecules are well separated by dilution, and will be the greatest in the fully solvated crystals of **2**·$2Et_2O$·$4CH_2Cl_2$, where intermolecular interactions mediated by π-stacking of aromatic rings and hydrogen-bonding via CH_2Cl_2 molecules were observed (see above).

AC Susceptibility Studies of Complex 2. In an ac susceptibility experiment, a weak field (typically 1−5 G) oscillating at a particular frequency is applied to a sample to probe the dynamics of its magnetization relaxation.[2,6,30] An out-of-phase ac susceptibility signal (χ_M'') is observed when the rate at which the magnetization of the sample relaxes (or reverses from "spin-up" to "spin-down") is close to the oscillation frequency of the applied ac field. Frequency-dependent χ_M'' signals have been observed in the ac susceptibility studies of all SMMs and are considered a diagnostic signature of the SMM property. In addition, ac magnetic susceptibility data can be employed to obtain the effective energy barrier (U_{eff}) for magnetization relaxation. Given that complex **2** appears to possess both of the criteria for single-molecule magnetism (a relatively large spin ground state and ZFS), ac susceptibility studies were performed in order to determine if it is indeed a SMM.

(30) Novak, M. A.; Sessoli, R. In *Quantum Tunnelling of Magnetization*, QTM '94; Gunther, L., Barbar, B., Eds.; Kluwer: Dordrecht, The Netherlands, 1995; pp 171−188.

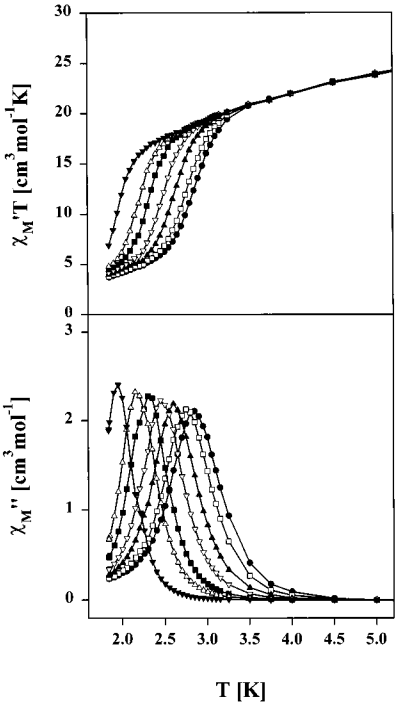

Figure 7. Plots of (top) the in-phase χ_M' signal as $\chi_M'T$ and (bottom) out-of-phase χ_M'' signal vs temperature for a powder sample of unsolvated complex **2** in a 3.5 G ac field oscillating at 1488 (●), 997 (□), 499 (▲), 250 (▽), 100 (■), 50 (△), and 10 (▼) Hz.

AC magnetic susceptibility measurements were performed on an unsolvated powder sample of **2** in a 3.5 G ac field oscillating at 10−1500 Hz in the 1.8−10 K range (Figure 7). The upper panel shows the χ_M' vs T plot, where χ_M' is the in-phase magnetic susceptibility, and the lower panel shows the χ_M'' vs T plot. The frequency-dependent decrease in the $\chi_M'T$ vs T plot at $T < 4$ K is consistent with the magnetization relaxation rate becoming comparable with the ac oscillation frequencies. This was confirmed by the concomitant appearance of a frequency-dependent out-of-phase (χ_M'') signal, which demonstrates that complex **2** is a SMM. The χ_M'' signal has a peak at ~2.7 K at a 997 Hz ac frequency, which is a temperature higher than those observed at this frequency for all previously reported SMMs that are not derived from $[Mn_{12}O_{12}(O_2CR)_{16}(H_2O)_x]$. Note that, at temperatures higher than those associated with the slow relaxation of magnetization, the $\chi_M'T$ vs T plot does not display a plateau, indicating that even at these low temperatures excited states are still populated. Extrapolation of this $\chi_M'T$ behavior to $T = 0$ K leads to a value of 16−25 $cm^3\ mol^{-1}$ K, corresponding to an $S = 6 \pm 1$ system with $g = 2$, consistent with the reduced magnetization results above.

To further investigate the effect of solvation on the magnetic behavior of complex **2**, ac measurements were also performed on **2**·$0.7CH_2Cl_2$, on a frozen solution of **2** in DMF (~1 mg in 0.3 cm^3), and on crystals of **2**·$2Et_2O$·$4CH_2Cl_2$.

Complex **2**·$0.7CH_2Cl_2$ displays ac behavior (Figure 8) similar to that of unsolvated **2** (Figure 7). The main difference is that the temperature at which the magnetization relaxation rate becomes comparable with the ac oscillation frequencies is lower for **2**·$0.7CH_2Cl_2$; that is, the decrease in $\chi_M'T$ and the appearance of a χ_M'' signal occur at lower temperatures. At 997 Hz, the χ_M'' signal has a peak at ~2.4 K for **2**·$0.7CH_2Cl_2$, compared to ~2.7 K for **2**. This difference is also apparent in the Arrhenius

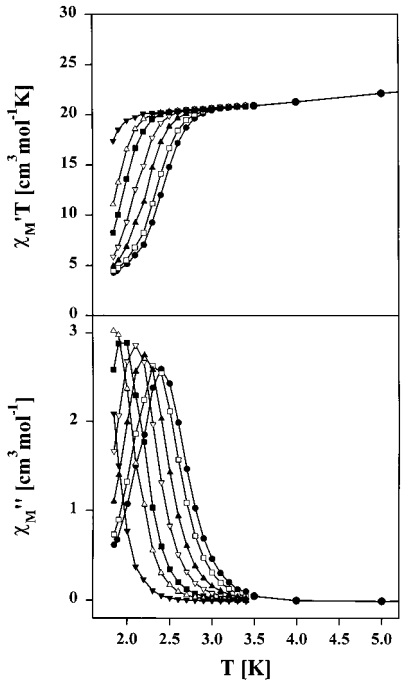

Figure 8. Plots of (top) the in-phase χ_M' signal as $\chi_M'T$ and (bottom) out-of-phase χ_M'' signal vs temperature for a powder sample of **2**·0.7CH_2Cl_2 in a 3.5 G ac field oscillating at 1488 (●), 997 (□), 499 (▲), 250 (▽), 100 (■), 50 (△), and 10 (▼) Hz.

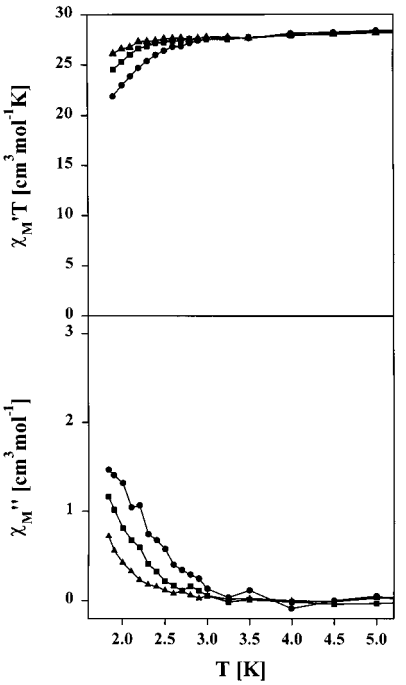

Figure 9. Plots of (top) the in-phase χ_M' signal as $\chi_M'T$ and (bottom) out-of-phase χ_M'' signal vs temperature for a frozen DMF solution of complex **2** in a 3.5 G ac field oscillating at 1488 (●), 250 (■), and 50 (▲) Hz.

plots (vide infra). In addition, the ac susceptibility behavior of **2**·0.7CH_2Cl_2 differs from that of unsolvated **2**, in that at temperatures higher than those associated with the slow relaxation of magnetization, the $\chi_M'T$ vs T plot does display a flatter plateau, perhaps consistent with reduced occupation of low-lying excited states. Extrapolation of this behavior to $T = 0$ leads to a value of $\chi_M'T \sim 20$ cm^3 mol^{-1} K, again consistent with $S = 6 \pm 1$.

The frozen solution of complex **2** in DMF also displays the ac susceptibility behavior of a SMM (Figure 9), with a frequency-dependent decrease in the $\chi_M'T$ vs T and a concomitant appearance of a frequency-dependent χ_M'' signal. However, in this case the temperature at which the magnetization relaxation rate becomes comparable with the ac oscillation frequencies is even lower than for **2**·0.7CH_2Cl_2. At the lowest temperature measured, 1.8 K, the χ_M'' signal, although displaying a frequency-dependent increase, does not exhibit a peak at even the highest frequency of 1500 Hz. Lower temperatures or higher frequencies are required in order to observe the peak positions. In addition, for the frozen solution of **2**, the $\chi_M'T$ vs T plot again displays a flatter plateau at temperatures higher than those associated with the slow relaxation of magnetization than that observed for unsolvated **2**. Extrapolation of this behavior to $T = 0$ leads to a value of $\chi_M'T \sim 27$ cm^3 mol^{-1} K, consistent with $S \sim 7$. In addition, this plot is relatively noisy for the reasons discussed above.

In contrast to the other forms of **2**, **2**·2Et_2O·4CH_2Cl_2 does not display ac susceptibility behavior consistent with a SMM. The $\chi_M'T$ value is near zero and there is no χ_M'' signal (see Supporting Information). The $\chi_M'T$ vs temperature data are similar to the χ_MT data measured by dc magnetic susceptibility, with both heading for 0 cm^3 mol^{-1} K at 0 K (see Supporting Information).

The ac magnetic susceptibility data measured for the four different forms of complex **2**, are essentially consistent with the dc magnetic susceptibility data. Unsolvated **2**, **2**·0.7CH_2Cl_2, and the frozen DMF solution of **2** all display frequency-dependent ac susceptibility behavior indicative of slow relaxation of the magnetization and single-molecule magnetism, thereby implying relatively high-spin ($S = 6$ or 7) ground states. In particular, the slow relaxation in the frozen solution of **2** provides clear evidence that complex **2** is a SMM and that the solid-state behavior is not due to long-range ordering or spin glass formation. However, the behavior is clearly very solvation-dependent, with this dependence most manifest in the temperature at which the slow relaxation becomes evident in the ac studies. Taking this solvent dependence to the extreme, complex **2**·2Et_2O·4CH_2Cl_2 appears not to be a SMM and both the ac and dc susceptibility data suggest either an $S \sim 0$ ground state or (more likely) a high-spin molecule with intermolecular antiferromagnetic interactions dominating the behavior at low temperatures. The latter has previously been observed for linked chains of tetranuclear Mn SMMs, although in that case the intermolecular interactions occur through the covalent bonds that link the discrete clusters.[31] Solvation dependence in SMM behavior has been observed in other compounds, although not quite in the same way as in the present case. The well-studied $[Mn_{12}O_{12}(O_2CR)_{16}(H_2O)_4]$ SMMs display solvation dependence in the form of "Jahn−Teller isomerism",[8a,32] in which the solvation stabilizes different orientations of some of the Mn^{III} Jahn−Teller axes, leading to χ_M'' signals in different temperature regimes depending on the particular Jahn−Teller isomer. Solvation dependence has also been reported for the SMM

(31) Yoo, J.; Nakano, M.; Krzystek, J.; Streib, W. E.; Brunel, L.-C.; Christou, G.; Hendrickson, D. N. Manuscript in preparation.

$[Mn_4(O_2CMe_3)_2(pdmH)_6][ClO_4]_2$, where the anhydrous form was found to possess an $S = 8$ ground-state spin while the hydrated form possesses an $S = 9$ ground state.[10] These differences were clearly evident in both the dc and ac magnetic susceptibility, although their origin remains uncertain. In the present case, the solvation dependence may be due to intermolecular interactions mediated by the solvent molecules, and for $\mathbf{2}\cdot 2Et_2O\cdot 4CH_2Cl_2$, these may result in intermolecular antiferromagnetic exchange interactions and long-range ordering that lead to the apparent magnetic susceptibility behavior of a ground-state $S = 0$ system. As the solvent is lost, the hydrogen-bonding network is lost, and the loss of crystallinity also diminishes the π-stacking interactions; thus, the behavior approaches that of isolated molecules that are SMMs. Taking the case to the opposite extreme, dissolution of the complex affords a system where the molecules are well isolated, again leading to the behavior of SMMs. This explanation is consistent with the observed ac and dc magnetic susceptibility behavior displayed by the four different forms of complex **2**. An alternative explanation is that solvate molecules in proximity to or interacting with the Mn_{12} complex stabilize structural forms with slight differences in bond distances and angles. It is believed that this type of effect causes the Jahn−Teller isomerism in the $[Mn_{12}O_{12}(O_2CR)_{16}(H_2O)_x]$ family, so it is not unreasonable that in a system such as the present one, where the spin ground state is the result of many competing pairwise exchange interactions, small differences in bond parameters could lead to large differences in the ground-state spin and/or the ZFS of the molecule, and thus have a significant effect on the SMM behavior. It must be emphasized that the exact origin of the differing magnetization relaxation rates of the various solvated forms of **2** remains uncertain, but that it is very clear that the magnetic properties of SMMs can be acutely sensitive to solvation level.

The data for **2** were analyzed further as follows. At the temperature of the χ_M'' vs T maximum, the relaxation rate equals the ac angular frequency (ω) and thus the relaxation rate ($1/\tau$) can be obtained from the relationship $\omega\tau = 1$.[30] Thus, measurement of the peak maxima at several frequencies provides $1/\tau$ vs T data and a kinetic analysis can be performed by use of the Arrhenius relationship:

$$\frac{1}{\tau} = \frac{1}{\tau_0}\exp(-U_{\text{eff}}/kT) \tag{3a}$$

$$\ln(1/\tau) = -U_{\text{eff}}/kT + \ln(1/\tau_0) \tag{3b}$$

This is the characteristic behavior for a thermally activated Orbach process,[33] where U_{eff} is the effective anisotropy energy barrier, k is the Boltzmann constant, and T is the temperature. A plot of $\ln(1/\tau)$ vs $1/T$ with data for complex **2** collected at the seven ac frequencies of Figure 7 is given in Figure 10, together with the data for $\mathbf{2}\cdot 0.7CH_2Cl_2$ from Figure 8. The error bars on the data points for unsolvated complex **2** represent data from many determinations to test the reproducibility and precision of the data. The least-squares fit to eq 3b for each set of data is shown as a solid line. From the slope and intercept were determined that $U_{\text{eff}} = 21.1$ cm^{-1} (30.3 K) and $1/\tau_0 = 4.0 \times 10^8$ s^{-1} for unsolvated complex **2** and $U_{\text{eff}} = 20.3$ cm^{-1} (29.1 K) and $1/\tau_0 = 1.7 \times 10^9$ s^{-1} for complex $\mathbf{2}\cdot 0.7CH_2Cl_2$. It is of considerable interest that the U_{eff} values are essentially the same for unsolvated **2** and $\mathbf{2}\cdot 0.7CH_2Cl_2$. To a first approximation, the energy barrier for relaxation is given by $U = S^2|D|$, for an integer spin system with axial symmetry, and $U \approx U_{\text{eff}}$ in the absence of quantum tunneling.[30] Thus, it seems that the S and D values are similar in the two forms of **2**, i.e., that the dodecanuclear complex is essentially conserved. This suggests that the solvation effects that cause the differing behavior for the different forms of **2** do not do so by altering the values of S or the anisotropy parameters. Instead, the different relaxation rates for the different solvation forms appear to be solely due to the different preexponential factors ($1/\tau_0$) in eq 3, modulated by the different environments and/or intermolecular interactions of the clusters. Experimentally, the $1/\tau_0$ values for unsolvated **2** and $\mathbf{2}\cdot 0.7CH_2Cl_2$ have been found to differ by a factor of 4 (4.0×10^8 and 1.7×10^9, respectively). Finally, use of the approximation that $U = S^2|D| \approx U_{\text{eff}}$ suggests a value of $D \approx -0.4$ to -0.6 cm^{-1} (-0.6 to -0.9 K), assuming $S = 6$ or 7.

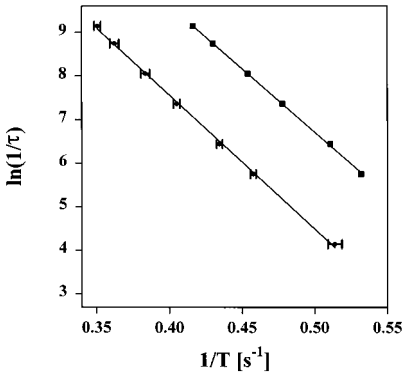

Figure 10. Plot of the natural logarithm of the relaxation rate [$\ln(1/\tau)$] vs the inverse of the temperature for a powder sample of unsolvated complex **2** (●) and a powder sample of $\mathbf{2}\cdot 0.7CH_2Cl_2$ (■). The solid lines represent least-squares fits of the data to the Arrhenius equation; see the text for fitting parameters.

More detailed ac susceptibility measurements were made on **2** to further investigate the nature of the magnetization relaxation processes. The ac susceptibility was measured at a constant temperature of 2.1 K on a sample of vacuum-dried unsolvated complex **2,** while the frequency of oscillation of the 3.5 G ac field was varied in the range 0.1−1500 Hz. For a single relaxation process, the χ_M' and χ_M'' behavior as a function of angular frequency (ω), is given by eqs 4 and 5, respectively:

$$\chi'(\omega) = \chi_s + \frac{(\chi_T - \chi_s)}{1 + \omega^2 t^2} \tag{4}$$

$$\chi''(\omega) = \frac{(\chi_T - \chi_s)\omega\tau}{1 + \omega^2 t^2} \tag{5}$$

where $\chi_s = \chi_{\omega\to\infty}$ is the adiabatic susceptibility, $\chi_T = \chi_{\omega\to 0}$ is the isothermal susceptibility, $\omega = 2\pi\nu$ is the angular frequency, and τ is the magnetization relaxation time. The isothermal

(32) (a) Sun, Z.; Ruiz, D.; Dilley, N. R.; Soler, M.; Ribas, J.; Folting, K.; Maple, M. B.; Christou, G.; Hendrickson, D. N. *Chem. Commun.* **1999**, 1973. (b) Aubin, S. M. J.; Sun, Z.; Eppley, H. J.; Rumberger, E. M.; Guzei, I. A.; Folting, K.; Gantzel, P. K.; Rheingold, A. L.; Christou, G.; Hendrickson, D. N. *Inorg. Chem.* **2001**, *40*, 2127. (c) Aubin, S. M. J.; Sun, Z.; Eppley, H. J.; Rumberger, E. M.; Guzei, I. A.; Folting, K.; Gantzel, P. K.; Rheingold, A. L.; Christou, G.; Hendrickson, D. N. *Polyhedron* **2001**, *20*, 1139.

(33) (a) van Duyneveldt, A. J. In *Magnetic Molecular Materials*; Gatteschi, D., Kahn, O., Miller, J., Palacio, F., Eds.; Kluwer Academic Publishers: London, 1991. (b) Abram, A.; Bleaney, B. *Electron Paramagnetic Resonance of Transition Ions*; Dover Press: Minneaola, NY, 1986.

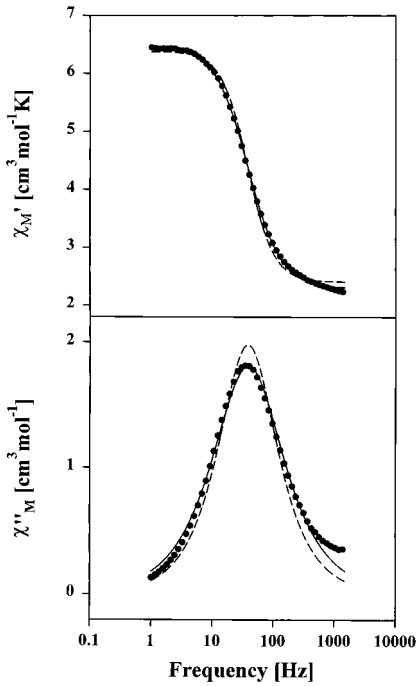

Figure 11. Plots of (top) χ_M' vs frequency and (bottom) χ_M'' vs frequency at 2.1 K for an unsolvated powder of complex **2**. The dashed lines are a least-squares fitting of the data to a single relaxation process as described by eqs 4 and 5; the solid lines are a least-squares fitting of the data to a distribution of single relaxation processes as described by eqs 6 and 7; see the text for the fitting parameters.

susceptibility, χ_T, is the dc susceptibility for paramagnets obeying the Curie law. For a distribution of single relaxation processes, the expressions for χ' and χ'' are given by eqs 6 and 7:[34a]

$$\chi'(\omega) = \chi_s + \frac{(\chi_T - \chi_s)[1 + (\omega\tau)^{1-\alpha}\sin(\alpha\pi/2)]}{1 + 2(\omega\tau)^{1-\alpha}\sin(\alpha\pi/2) + (\omega t)^{2(1-\alpha)}} \quad (6)$$

$$\chi''(\omega) = \chi_s + \frac{(\chi_T - \chi_s)(\omega\tau)^{1-\alpha}\cos(\alpha\pi/2)}{1 + 2(\omega\tau)^{1-\alpha}\sin(\alpha\pi/2) + (\omega t)^{2(1-\alpha)}} \quad (7)$$

where α is a value between 0 and 1 and gauges the width of the distribution. When $\alpha = 0$, eqs 6 and 7 reduce to eqs 4 and 5, respectively, describing a single relaxation process. A distribution of single relaxation processes as given in eqs 6 and 7 has been used extensively to describe the ac susceptibility data for spin glasses and also for the SMM $[Mn_{12}O_{12}(O_2CEt)_{16}(H_2O)_4]^-$.[6c,34]

The data for complex **2** are presented in Figure 11 as plots of χ_M' vs frequency and χ_M'' vs frequency. The dashed lines result from least-squares fitting of the data to a single relaxation process, as described by eqs 4 and 5, to give $\chi_s = 2.41$ cm^3 mol^{-1}, $\chi_T = 6.38$ cm^3 mol^{-1}, and $\tau = 4.23 \times 10^{-3}$ s. Considerably improved fits are obtained when the data are fit to a distribution of single relaxation processes (eqs 6 and 7). This gives $\chi_s = 2.30$ cm^3 mol^{-1}, $\chi_T = 6.48$ cm^3 mol^{-1}, $\alpha = 0.206$, and $\tau = 4.20 \times 10^{-3}$ s. The fitting parameters obtained from the two different fitting schemes are similar and, in particular, the resulting relaxation times (τ) are very close. The data for complex **2** are also given in Figure 12 as a Cole−Cole or Argand plot of χ_M' vs χ_M'', which gives information on the number of distinct relaxation processes that are occurring. A symmetric Argand plot is indicative of a single relaxation process, as is the case for complex **2**. Again it is apparent that fitting the data to a distribution of single relaxation processes (solid line) results in a substantially better fit than fitting the data to a single relaxation process (dashed line). From these data it can be concluded that only a single relaxation process is occurring for unsolvated complex **2**. Further, there is a distribution in this single relaxation process. This is similar to what was previously observed for $[Mn_{12}O_{12}(O_2CEt)_{16}(H_2O)_4]^-$ and probably results from molecules in the powder sample exhibiting a distribution in effective energy barriers, i.e., a narrow range in U_{eff} values due to a distribution of environments of the molecules.[6c] This would lead to a distribution of ZFS parameters, thus affecting the potential-energy barrier height.

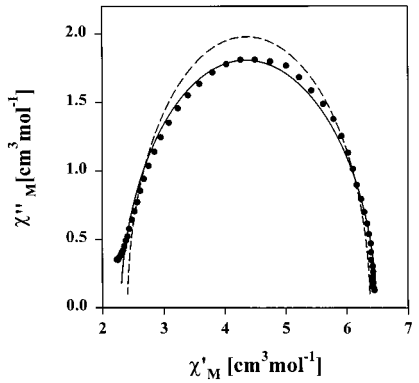

Figure 12. Argand plot of χ_M' vs χ_M'' at 2.1 K for an unsolvated powder of complex **2**. The dashed line is a least-squares fitting of the data to a single relaxation process as described by eqs 4 and 5. The solid line is a least-squares fitting of the data to a distribution of single relaxation processes as described by eqs 6 and 7; see the text for the fitting parameters.

Magnetochemistry of Complexes 3 and 4. Variable-temperature dc susceptibility measurements were performed on powder samples of complexes **3** and **4**, restrained in eicosane to prevent torquing. Almost identical behavior was observed, with the $\chi_M T$ value increasing slightly from 38.0 and 38.3 cm^3 mol^{-1} K at 300 K to 39.0 and 39.4 cm^3 mol^{-1} K at 200 K before steadily decreasing to 1.5 and 2.1 cm^3 mol^{-1} K at 1.8 K for **3** and **4**, respectively (see Supporting Information). The spin-only ($g = 2$) value for a noninteracting $Mn^{II}_2Mn^{III}_{10}$ is 38.8 cm^3 mol^{-1} K, indicating significant antiferromagnetic interactions, and the gradual decrease of $\chi_M T$ to ~0 cm^3 mol^{-1} K at 0 K is suggestive of $S \sim 0$ ground states. Magnetization data were collected in the ranges 10−50 kG and 1.8−4.0 K for complexes **3** and **4**. As for complex **2**, it was not possible to obtain a good fit for these data assuming that only one spin state is populated in this temperature range. This suggests that low-energy excited states are probably also populated for complexes **3** and **4**. Similar behavior has been observed previously for large molecules with S = 0 ground states.[27,35] AC susceptibility measurements were also performed on complexes **3** and **4** with a 3.5 G ac field oscillating at 997 Hz. Like the dc data, the ac data are almost identical for the two complexes. In addition, they are essentially superimposable with

(34) (a) Cole, K. S.; Cole, R. H. *J. Chem. Phys.* **1941**, *9*, 341. (b) Chamberlin, R. V.; Mozurkewich, G.; Orbach, R. *Phys. Rev. Lett.* **1984**, *52*, 867. (c) Weiss, G. H.; Dishon, M.; Long, A. M.; Bendler, J. T.; Jones, A. A.; Inglefield, P. T.; Bandis, A. *Polymer* **1994**, *35*, 1880.

(35) Squire, R. C.; Aubin, S. M. J.; Folting, K.; Streib, W. E.; Christou, G.; Hendrickson, D. N. *Inorg. Chem.* **1995**, *34*, 6463.

the dc data, except at the very lowest temperatures, and appear to be heading for $\chi_M T = 0$ cm^3 mol^{-1} K at 0 K, suggesting an $S = 0$ ground state for both complexes **3** and **4** (see Supporting Information).

Concluding Comments

The reaction of $(NBu^n_4)[Mn_8O_6Cl_6(O_2CPh)_7(H_2O)_2]$ (**1**) with hmpH and hepH affords the structurally related compounds $[Mn_{12}O_8Cl_4(O_2CPh)_8(hmp)_6]$ (**2**) and $[Mn_{12}O_8Cl_4(O_2CPh)_8(hep)_6]$ (**3**), respectively. Reaction of **3** with HBr gives $[Mn_{12}O_8Br_4(O_2CPh)_8(hep)_6]$ (**4**). Complexes **2**−**4** have been structurally characterized and represent a new structural type. Complexes **2** and **3** possess isomeric cores, resulting in differing arrangements of the peripheral ligands, while **4** is essentially isostructural with **3**. Although these complexes possess related structures, they display markedly different magnetochemical behavior, indicative of a high ground-state spin for **2** and ground-state spin of 0 for **3** and **4**. The ground-state spin results from a combination of all of the individual pairwise magnetic exchange interactions, which differ between the two structures.

Complex **2** appears to possess a ground-state spin of 6 or 7. A more precise determination is difficult, owing to the presence of Mn(II) and the resulting occupation of low-lying excited states even at low temperatures. Similarly, the axial zero-field splitting parameter cannot be precisely determined but appears to be in the range −0.4 to −0.6 cm^{-1} (−0.6 to −0.9 K). As a result of the relatively large values of S and $|D|$, complex **2** is a SMM, with frequency-dependent peaks evident in the out-of-phase ac susceptibility plot for unsolvated complex **2**, indicative of slow relaxation of the magnetization. These signals occur at temperatures higher than those observed for all previously reported single-molecule magnets that are not derived from $[Mn_{12}O_{12}(O_2CR)_{16}(H_2O)_x]$. However, the behavior displays a significant dependence on the solvation of the complex. Partially solvated **2**·0.7CH_2Cl_2 and a frozen solution of **2** still display frequency-dependent peaks in the out-of-phase ac susceptibility plots, although the temperatures at which these signals are observed are lower than for the unsolvated form. In contrast, fully solvated **2**·2Et_2O·4CH_2Cl_2 does not display slow relaxation of the magnetism, instead showing apparent behavior consistent with an $S = 0$ system. Significantly, slow relaxation of the magnetization is still observed in the frozen solution of **2**, indicating that **2** is indeed a SMM.

An analysis of the ac susceptibility data by use of the Arrhenius relationship gives values of $U_{eff} = 21.1$ and 20.3 cm^{-1} (30 and 29 K) for unsolvated and partially solvated complex **2**, respectively. This demonstrates that the solvation dependence of the relaxation rate is not due to the solvate molecules altering the activation energy barrier, as is proposed to occur in the Jahn−Teller isomerism of $[Mn_{12}O_{12}(O_2CR)_{16}(H_2O)_x]$, but to changes to the Arrhenius preexponential factor. Furthermore, an Argand plot of the ac susceptibility data for unsolvated complex **2** clearly indicates that only one relaxation process is occurring. Thus, the solvation dependence has been interpreted in terms of the presence of various degrees of intermolecular antiferromagnetic exchange interactions mediated by the hydrogen-bonding network and π-stacking of aromatic rings, leading to long-range antiferromagnetic ordering in the fully solvated form. There is evidence for both of these types of interactions in the X-ray structure of complex **2**·2Et_2O·4CH_2Cl_2.

It is anticipated that further characterization of this system to more precisely determine the values of S and D and to fully elucidate the nature of the solvation dependence, will prove difficult. This is due to the occupation of low-lying excited states, even at very low temperatures, which will hinder HFEPR measurements. In addition, the crystals lose crystallinity as they rapidly lose solvent. Hence any measurement technique that requires intact single crystals, such as single-crystal HFEPR or micro-SQUID studies, can only be performed on the fully solvated species, which is the form of **2** that does not display SMM behavior. The results presented herein should serve as a warning of the possible extreme sensitivity of SMM behavior to factors such as solvation.

Acknowledgment. This work was supported by National Science Foundation grants to D.N.H. and G.C.

Supporting Information Available: X-ray crystallographic files in CIF format for complexes **2**, **3,** and **4** and various structural and magnetism figures as mentioned in the text. This material is available free of charge via the Internet at http://pubs.acs.org.

JA012403K